Journal of Molecular Catalysis A: Chemical 333 (2010) 54–68

Contents lists available at ScienceDirect

Journal of Molecular Catalysis A: Chemical

journal homepage: www.elsevier.com/locate/molcata

Nanoscale surface study and reactions mechanism of 2-butanol over the γ-alumina (1 0 0) surface and nanochannel: A DFT study

Hossein A. Dabbagh [a,*], Mehdi Zamani [a], Burtron H. Davis [b]

[a] Catalysis Research Laboratory, Department of Chemistry, Isfahan University of Technology, Isfahan 841548311, Iran
[b] 2540 Research Park Drive, Center for Applied Energy Research, University of Kentucky, Lexington, KY 40511, USA

ARTICLE INFO

Article history:
Received 5 June 2010
Received in revised form
20 September 2010
Accepted 23 September 2010
Available online 1 October 2010

Keywords:
γ-Alumina (1 0 0) surface
Nanochannel
anti/syn E2-elimination
Conformational analysis
DFT

ABSTRACT

The mechanism of adsorption, dissociation, hydrogen-shift, dehydration and dehydrogenation of adsorbed (*R*)- and (*S*)-2-butanol over the dehydroxylated (1 0 0) surface and nanochannel of γ-alumina defect spinel structure was computed by density functional theory (DFT). To test the asymmetric property of this surface by conformational analysis of adsorbed (*R*)- and (*S*)-2-butanol was investigated. Computed conformational analysis indicates that the (*S*)-isomer bond with the surface is stronger than the (*R*)-isomer. Steric interactions between adsorbed alcohol and catalyst surface appear to be more important than intramolecular steric constraints present within the alcohol conformations. Mulliken atomic charges predict that selected basic sites (O_{a-h}) play a major role in elimination reactions. E2 elimination with synclinal transition state was comparable with E2 antiperiplanar transition state. The activation energy for elimination of a β-hydrogen from the 2-butanol conformers increases with increasing the distance between β-hydrogen and basic sites. The formation of alkenes (thermodynamic products) is favored over the formation of ketone (kinetic product).

1. Introduction

In recent years, much attention has been paid to prepare and characterize nanosize alumina (e.g., nanoparticles [1], fullerenes [2], nanotubes [3], nanocapsules [4], nanowires [5], nanotrees [5], nanorods [6], nanochannels [7], mesoporous [8] and nano-porous [9]) materials. These nanostructures are similar in composition but different in shape. Many experimental and theoretical works have investigated the structure and phase stability of transition aluminas [10–14]. The conceptions which describe the surface properties of different aluminas are quite interesting. Qualitative quantum chemical calculations have recently developed two models of γ-alumina, a cluster model [15–25] and a periodic slab on the surface [26–43].

The bulk structure of γ-alumina is closely related to that of magnesium spinel (MgO, Al_2O_3). A spinel has 24 cations (Mg or Al) and 32 oxygen atoms in the unit cell of a cubic lattice. Because Al is trivalent and Mg is divalent, the number of Al atoms in the spinel structure of γ-alumina is smaller than the number of cations in the spinel. Therefore, to reach the proper stoichiometry some of the cation sites in the spinel structure must be empty [27]. Ionescu et al. [28–30] provided an exhaustive structural and electronic properties studies of γ-Al_2O_3 ideal and defect spinel structures. The correlation between the positions of the cation vacancies and the energies of the possible structures has been examined by several authors. Some studies indicate the vacancies are at tetrahedral (T_d) sites, others at octahedral (O_h), and several show different proportions of tetrahedral and octahedral vacancies. Streitz and Mintmire [31] investigated the O_h vacancy with lower potential energy, but only by 0.53 eV per vacancy. Taniike et al. [32] found that an O_h vacancy was favored over T_d vacancy by 1.1 eV. Vijay et al. [27] and Gutierrez et al. [33] reported higher stability for the octahedral vacancy than tetrahedral vacancy. Mo et al. [34] found that the energy required for moving vacant spinel site from O_h to T_d site is 3.7 eV.

Sohlberg et al. supported the presence of various amounts of hydrogen within the bulk structure of spinel γ-alumina [19–22]. They showed that γ-alumina is, in fact, a sequence of hydrogen-containing compounds of the form $H_{3m}Al_{2-m}O_3$. The terminus of the sequence is the widely promoted defect spinel structure. This idea has been reported by others. For instance, Handzlik et al. [25] used four types of alumina (1 0 0) clusters ($Al_6O_{22}H_{26}$, $Al_8O_{26}H_{28}$, $Al_{10}O_{30}H_{30}$ and $Al_{12}O_{34}H_{32}$) and De Vito et al. [24] used the $Al_3O_9H_{10}^+$ cluster model for their calculations, whereas Wolverton and Hass [11] indicated that hydrogen spinel is thermodynamically unstable with respect to the decomposition into an anhydrous defect spinel plus boehmite. Recently, Raybaud and co-workers reported a complete nonspinel structure based on molecular dynamic simulations and DFT calculations of the dehydration of boehmite [36–39]. This model showed good agreement

* Corresponding author. Tel.: +98 311 391 3257; fax: +98 311 391 2350.
E-mail address: dabbagh@cc.iut.ac.ir (H.A. Dabbagh).

1381-1169/$ – see front matter © 2010 Elsevier B.V. All rights reserved.
doi:10.1016/j.molcata.2010.09.016

with experimental data in terms of structural parameters and OH vibrational frequencies [24]. Nelson et al. [44,45] performed DFT and simulated XRD calculations for identification of three different spinel-related γ-alumina structures (fully and partly hydrogenated structures and defect spinel) versus nonspinel models. They concluded that the spinel related structure model is better than the nonspinel model of the bulk structure of γ-Al_2O_3. This idea immediately was criticized by Paglia et al. [46]. They showed that a non-spinel structure matches data from neutron diffraction experiments [46–48]. Recently, a single crystal X-ray diffraction study of γ-Al_2O_3 was reported by Smrcok et al. [49]. Refined occupancy parameters indicated that, in addition to the ideal spinel positions, approximately 6% of Al ions also occupy non-spinel positions.

Theoretical investigations of the adsorption on γ-alumina have focused mostly on Lewis acidity of the surface [36], and the reactivity with water [15,16,18,28,29], hydrogen sulfide [15,28,29], carbon monoxide [15,29], ammonia [16], pyridine [16,36], hydrogen chloride [17], alkenes [19,23], and alkanes [20]. Also several papers have been reported for the adsorption of alcohols over the γ-alumina [24,42,43,50]. De Vito et al. [24] have studied the adsorption of methanol. They concluded that the methanol adsorbs on a tetrahedral aluminum ion forming a covalent bond. Cai and Sohlberg [42] computed the adsorption of methanol, ethanol, propanol, and iso-propanol over the γ-alumina (1 1 0) surface. They have shown that all four alcohols considered, chemisorb to the alumina surface when they come sufficiently close to surface with suitable orientation. Feng et al. [43] presented a detailed theoretical study on isopropanol adsorption on both clean and hydrated γ-alumina (1 0 0) and (1 1 0) surfaces. They have considered all possible adsorption configurations in their calculation. Recently, we examined the adsorption mechanism of (*R*)-, (*S*)-2-octanol and (*R*)-, (*S*)-1,2-diphenyl-2-propanol (DPP) conformers over the dehydroxylated (1 0 0) and (1 1 0) surfaces of defect spinel γ-alumina at DFT level of theory [50]. The main specific feature of these surfaces is the asymmetric property. This feature stems from the holes and vacancies of defect γ-alumina bulk structure. This model predicts that (1 0 0) and (1 1 0) surfaces with the adsorbed chiral alcohol show diasteroselective property. In addition, we reported a lower adsorption energy for the adsorbed 2-octanol in comparison with that of adsorbed DPP. The phenyl groups of DPP with a high electron density adsorb more strongly over the surface than the long chain of 2-octanol. A brief discussion was presented describing the transition states and correlation between the activation energy and the distances of basic sites of alumina and eliminable hydrogens (β, β′ and β″) of 2-butanol.

In this study we examined the asymmetric property of the surface by conformational analysis of adsorbed (*R*)- and (*S*)-2-butanol over (1 0 0) surface and nanochannel of defect spinel structure at DFT/BLYP (Becke–Lee–Yang–Parr) [51,52] level of calculation. Then the stereochemistry of elimination, mechanism of dehydration, dehydrogenation and hydrogen shift were investigated. The main goals of the present study which outstand previous published papers, are as following: First, the analysis of structure and asymmetric properties of (1 0 0) surface of defect spinel γ-alumina. Second, study of adsorption behaviors of chiral alcohol (2-butanol) stereo isomers and their conformers over the surface. Third, computational analysis of the reaction mechanisms of a secondary alcohol over (1 0 0) surface γ-alumina. Finally, experimental and theoretical findings were compared. To the best of our knowledge, there is no theoretical work reported on these issues to this date.

2. Computational details

DFT calculations were performed using the DMOL^3 program [53,54]. The double numerical plus polarization function (DNP) and BLYP generalized gradient approximation were used in all calculations. It should be noted that the DNP basis set includes a double-zeta quality basis set that added a p-type and d-type polarization function to hydrogen and heavier atoms, respectively; and it is equivalent to 6-31G** Gaussian basis sets [55]. Each basis function is restricted to a cutoff radius of 4.5 Å. Effective core potentials (ECP) were used to treat the core electrons and a k-point set separation of 0.07 $Å^{-1}$. The tolerance of the energy change was set for all calculations to 1.0e−5 Ha (≈0.006 kcal mol^{-1}). All energies in this paper were reported by two decimal significant digits.

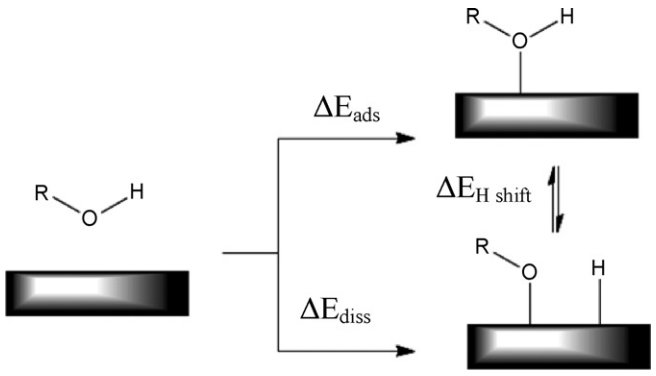

Scheme 1. The adsorption/dissociation pathways for reaction of 2-butanol over (1 0 0) surface.

In this study, the molecular adsorption of 2-butanol molecule for the dehydroxylated surface was investigated (generally aluminum hydroxides calcined at 600 °C show small number of hydroxyl moiety [50]). This surface can play an important role at high temperatures.

The selected 2-butanol conformers are called synclinal–antiperiplanar (sc–ap), synperiplanar–anticlinal (sp–ac), synclinal–synclinal (sc–sc), anticlinal–synperiplanar (ac–sp), antiperiplanar–synclinal (ap–sc) and anticlinal–anticlinal (ac–ac) according to the torsion angle between CH_3/CH_3 and CH_3/OH groups (Fig. 4). It should be noted that based on the nomenclature in organic chemistry [56] the sp, sc, ac and ap terms are defined for 0–30°, 30–90°, 90–150° and 150–180° torsion angles.

The adsorption energy (ΔE_{ads}) of the 2-butanol molecule is calculated as

$$\Delta E_{ads} = E_{(\text{adsorbed 2–butanol on surface})} - E_{(\text{2-butanol})} - E_{(\text{surface})}$$

$E_{(\text{adsorbed 2-butanol on surface})}$ refers to the energy of the system which is formed by an adsorbed 2-butanol molecule and the surface. $E_{(\text{2-butanol})}$ and $E_{(\text{surface})}$ refer to the energy of an isolated 2-butanol molecule and the bare surface (Scheme 1). A negative energy corresponds to a stable molecule-surface system.

In the case of chemisorption, when the 2-butanol molecule is exothermically dissociated on the surface, the dissociation energy (ΔE_{diss}) is defined as

$$\Delta E_{diss} = E_{(\text{dissociated 2–butanol on surface})} - E_{(\text{2-butanol})} - E_{(\text{surface})}$$

where $E_{(\text{dissociated 2-butanol on surface})}$ refers to the energy of the system formed by dissociation of the molecule on the surface (Scheme 1).

The third energy is called H shift energy ($\Delta E_{\text{H shift}}$) and is defined as

$$\Delta E_{\text{H shift}} = E_{(\text{adsorbed 2-butanol on surface})} - E_{(\text{dissociated 2-butanol on surface})}$$

This energy refers to the dissociation that occurs after physisorbtion (Scheme 1). Adsorption, dissociation, and H shift energies for adsorbed (*R*)- and (*S*)-2-butanol conformers over (1 0 0) surface are summarized in Table 1.

Table 1
Selected bond lengths, bond angles and Mulliken atomic charges for clean γ-alumina (1 0 0) surface, free 2-butanol and after adsorption of 2-butanols along with their adsorption, dissociation and H shifts energies calculated at BLYP/DNP level of theory.[a]

Entry	(1 0 0) Surface (free 2-butanol)[c]	(*S*)-2-Butanol		(*R*)-2-Butanol	
		(sc–ap) conformer[b]	(sc–sc) conformer[b]	(ap–sc) conformer[b]	(sc–ap) conformer[b]
Bond lengths (Å)					
Al_c–O_a	1.875	1.897	1.903	1.898	1.895
Al_c–O_d	1.877	1.890	1.884	1.886	1.888
Al_c–O_c	1.919	1.946	1.961	1.954	1.955
Al_c–O_e	1.921	1.952	1.941	1.940	1.941
Al_e–O_g	1.876	1.881	1.886	1.885	1.887
Al_e–O_c	1.922	1.924	1.911	1.918	1.913
Al_e–O_e	1.921	1.901	1.909	1.908	1.908
Al_e–O_b	1.920	1.926	1.924	1.929	1.928
Al_e–O_a	1.879	1.869	1.869	1.867	1.869
Al_e–O_d	1.878	1.876	1.874	1.874	1.874
Al_c–$O_{alcohol}$	–	2.054	2.067	2.075	2.070
C–$O_{alcohol}$	(1.457)[c]	1.489	1.495	1.494	1.491
H–$O_{alcohol}$	(0.973)[c]	0.977	0.977	0.974	0.976
H–O_c	–	2.625	2.651	2.644	2.768
H–O_a	–	2.750	2.682	2.813	2.713
Bond angles (°)					
O–Al_c–O (external)	98.594, 98.608	98.961, 98.552	99.387, 98.214	99.382, 97.962	99.282, 98.082
O–Al_c–O (internal)	81.642	80.400	80.524	80.591	80.609
O–Al_e–O	81.565	81.501	81.648	81.705	81.657
Al_e–O–Al_c	99.229	97.633	97.679	97.708	97.650
$O_{alcohol}$–Al_c–O_a	–	92.238	91.096	92.037	91.728
$O_{alcohol}$–Al_c–O_c	–	86.623	86.163	86.687	87.179
$O_{alcohol}$–Al_c–O_d	–	99.091	98.799	98.117	98.228
$O_{alcohol}$–Al_c–O_e	–	93.726	94.365	93.943	94.069
(C–O–H) alcohol	(107.685)[c]	108.566	108.839	110.242	110.701
C–$O_{alcohol}$–Al_c	–	127.248	126.501	138.444	134.024
H–$O_{alcohol}$–Al_c	–	102.187	101.118	104.017	104.387
Mulliken charges					
$O_{alcohol}$	(−0.49)[c]	−0.56	−0.56	−0.56	−0.57
$H_{alcohol}$	(0.23)[c]	0.27	0.27	0.27	0.27
Al_c	1.385	1.55	1.55	1.56	1.55
Al_e	1.385	1.34, 1.38	1.34, 1.39	1.41, 1.39	1.41, 1.39
O_a	−0.944	−0.98	−0.98	−0.98	−0.98
O_b	−0.974	−0.98	−0.99	−0.98	−0.98
O_C	−0.974	−1.00	−0.99	−1.00	−0.99
O_d	−0.944	−0.98	−0.96	−0.98	−0.98
O_e	−0.974	−0.99	−0.99	−0.99	−0.99
O_f	−0.944	−0.95	−0.95	−0.95	−0.95
O_g	−0.944	−0.95	−0.95	−0.96	−0.95
O_h	−0.974	−0.98	−0.98	−0.98	−0.98
Energies (kcal mol^{-1})					
Adsorption	–	−29.95	−29.93	−28.15	−29.11
Disso. of complex via O_a	–	−35.14	−35.12	−31.93	−35.24
Disso. of complex via O_C	–	−19.12	−18.17	−17.47	−16.92
H-shift via O_a	–	−6.83	−5.18	−3.78	−6.14
H-shift via O_c	–	9.19	11.76	10.68	12.19
E_a for H-shift via O_a	–	69.34	69.00	70.92	71.28
E_a for H-shift via O_c	–	13.56	20.72	19.54	21.89

[a] Al_c is the central penta-coordinated aluminum atom in the surface that after adsorption of alcohol changes to hexa-coordination. Al_e is penta-coordinated aluminum atom at both edge of Al_c over (1 0 0) surface, see Figs. 1 and 5. All O_{a-h} in the alumina surface is three-coordinated.
[b] Optimized geometry of synclinal–antiperiplanar (sc–ap), synclinal–synclinal (sc–sc) and antiperiplanar–synclinal (ap–sc) conformers of 2-butanol is shown in Fig. 4.
[c] Value in parenthesis is related to free alcohol before adsorption.

To determine the activation energy (E_a) for a specific reaction path, a transition state was identified by the complete linear synchronous transit (LST) and the quadratic synchronous transit (QST) methods. Simulation of all reactions was performed under thermal condition.

3. Results and discussion

3.1. Optimized structure of γ-alumina (1 0 0) surface and nanochannel

Since previous evidence had proposed that the (1 0 0) and (1 1 0) planes were the most catalytically active and the (1 1 1) surface was not an active one [57], we focused our studies on the (1 0 0) surface. Studying of (1 1 0) surface is the subject of another investigation. The (1 0 0) surface orientation from defect spinel γ-alumina, based on the earlier models [28–30,58], were cleaved, as previously reported in Ref. [50]. We imposed a vacuum of 15 Å between slabs in the direction of the crystal lattice, perpendicular to the surface plane, and periodically repeated the unit cell through space. To speed up our calculations, we selected five layers of atoms (containing 40 atoms, $Al_{16}O_{24}$) while the two bottom layers of the slab was constrained (Fig. 1a). Both aluminum and oxygen atoms are present on these surfaces; aluminum atoms (Al_e and Al_c) are Lewis acid sites, whereas oxygen atoms (O_a–O_h) are Brønsted basic sites. In this model any of these sites may play

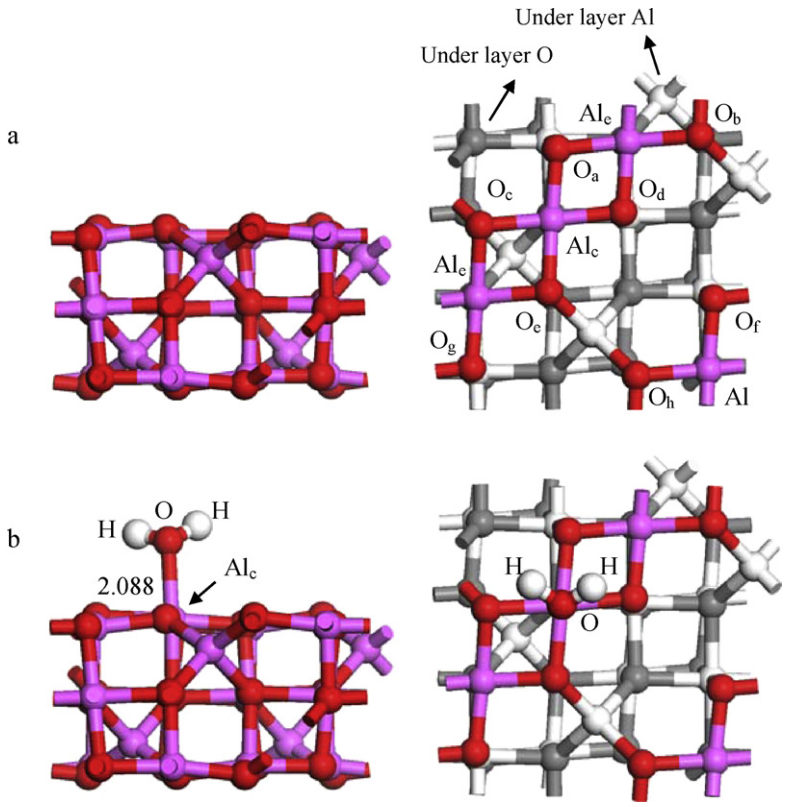

Fig. 1. Optimized geometry of γ-alumina clean (1 0 0) surface (a) and after water adsorption (b). Side view (left), top view (right). The under layers Al and O atoms of alumina are displayed by white and gray colors, respectively.

a role in the elimination process. It is possible for several sites to have different catalytic properties toward alcohol dehydration, both with respect to activity and selectivity. The upper layer of the (1 0 0) surface is formed by penta-coordinated aluminum (Al_V) and three-coordinated oxygen atoms (O_{III}), while in the middle layer aluminum atoms retain hexa (Al_{VI}), and tetra (Al_{IV}) coordinate geometry and oxygen atoms tetra coordinate (O_{IV}) geometry. The penta-coordinated aluminum atoms of the alumina surface are stronger Lewis acids than hexa(fully)-coordinated aluminum atoms. Lewis acidity of tetra-coordinated aluminum atoms has attracted less attention in the literature [24]. Bond lengths of Al_{IV} and Al_{VI} atoms with O_{IV} atoms in the fixed and relaxed layers are 1.844, 1.930, 1.828, and 1.991 Å. Bond lengths between Al_V and O_{III} atoms of relaxed layer are 1.875–1.922 Å (Table 1).

The correct choice of selecting (1 0 0) surface was validated by comparing the calculated value of adsorption energy (−19.94 kcal mol^{-1}) of water on the Al_c site of surface (Fig. 1b) with the initial heat of adsorption measured by microcalorimetric experiment (−19.83 kcal mol^{-1} [59]). The domain of previous theoretical adsorption energy of water on γ-alumina (1 0 0) surface extended from −25.56 to −44.92 kcal mol^{-1}. These results were obtained by quantum chemical methods on clusters that modeled different surface sites or periodic slabs [15,16,18,28,29].

Platelet like nanosized γ-alumina particles with (1 0 0), (1 1 0) and (1 1 1) faces joined together and made the γ-alumina supper cells [36,60]. This model was extended for the formation of nanochannels, when the pores and vacancies were generated between the platelets (Fig. S1, supporting information). Each (1 0 0) nanochannel ($Al_{32}O_{48}$) was composed of two platelet like nanosized γ-alumina (1 0 0) surfaces containing 40 atoms (Fig. 2). Geometry optimization of nanochannels was performed without any constraints. The relative energy of a nanochannel as a function of the distances between two platelet (1 0 0) layers is shown in Fig. 2. The curve of pure nanochannel (♦) has the lowest energy minimum at the distance of 4 Å (Fig. 2a). The distance between the layers must be at least 8 Å (Fig. 2b and c) for the doped (*S*)-2-butanol (sc–ap conformer) to achieve the minimum energy (curve ▲).

3.2. Conformational analysis of adsorbed (R)- and (S)-2-butanol on the γ-alumina (1 0 0) surface

One conformer of (*S*)-2-butanol (sc–ap conformer) was selected to investigation of the global energy minimum for different positions of molecule over Al_c site of γ-Al_2O_3 (1 0 0) surface by rotation about $O_{alcohol}$–Al_c bond from −100 to +100° (out of this range, the 2-butanol molecule leaves the vacuum slab). The molecular energy profile versus the O_d–Al_c–$O_{alcohol}$–C2 (Φ) dihedral angle and the optimized geometry of the main configurations are shown in Fig. S2. The structure showed in Fig. S2(e), in which hydroxyl group of 2-butanol is located at the central position of Al_c site (Φ = 6.861°), is the global energy minimum among all the other configurations. Therefore, this geometry was selected for the further investigations. The structure showed in Fig. S2(c) (Φ = −23.66°) is the second lowest-lying configuration with a relative energy of 0.20 kcal mol^{-1}. The structure showed in Fig. S2(g) (Φ = 43.128°) is the next configuration being 0.85 kcal mol^{-1} above the configuration shown in Fig. S2(e). Other configurations are less stable.

Conformational analysis of free 2-butanol and adsorbed (*R*)- or (*S*)-isomers over the (1 0 0) γ-Al_2O_3 surface (Al_c site) was performed by rotation about the C(2)–C(3) bond of $CH_3C(3)$–C(2)GCH_3 (G = OH, –Al_2O_3) from −180° to 180° (Fig. 3). Intramolecular interaction of 2-butanol influences the energy of the rotamers (with small deviation) which produce a typical potential energy scan (PES) plot (Fig. 3, top). However, both intramolecular and intermolecular interactions (between alcohol and the surface) have a pronounced effect on the rotamer energy (with large deviation) of

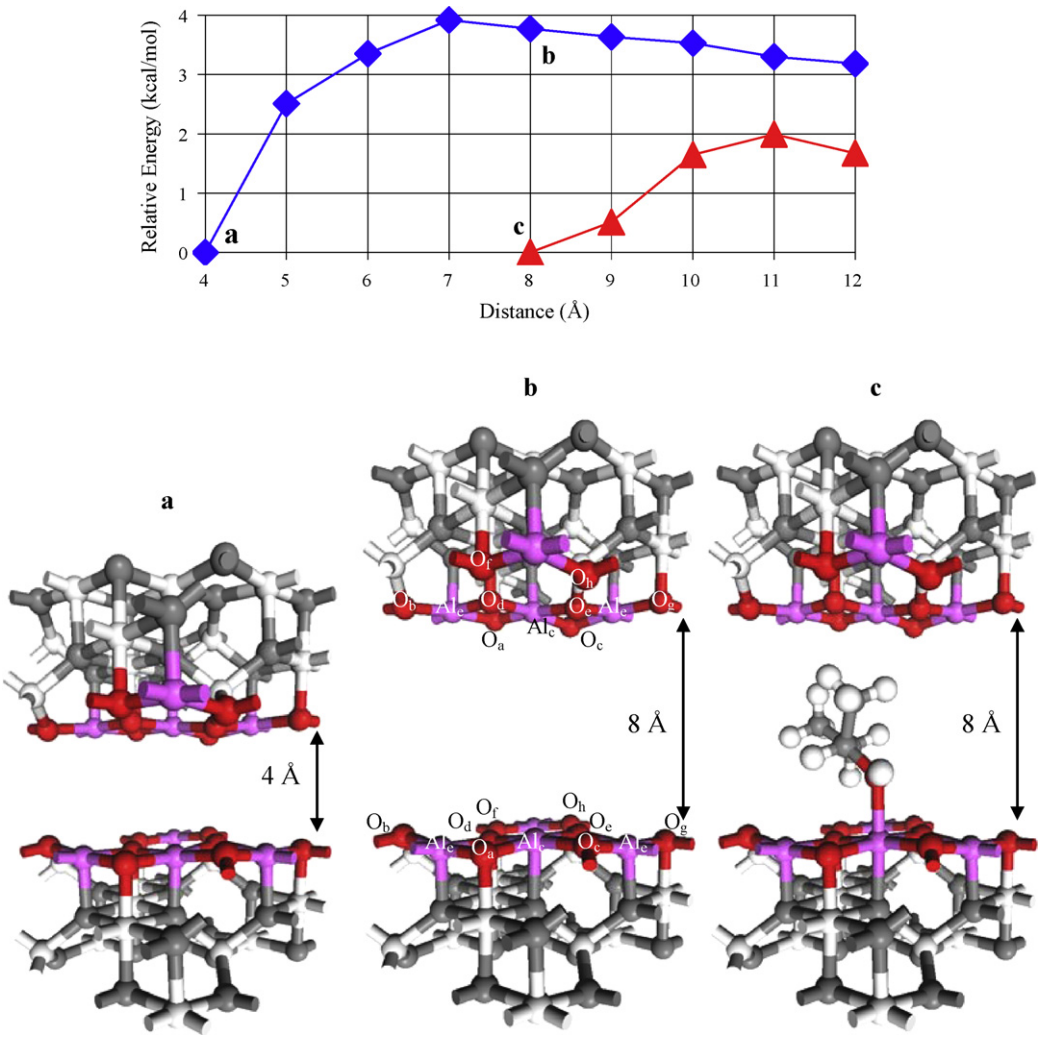

Fig. 2. Relative energy of γ-alumina (1 0 0) nanochannel before (♦) and after (▲) adsorption of (*S*)-2-butanol (sc–ap conformer) over Al_c site versus the distance between two platelet (1 0 0) layers (top) and the optimized geometry of the main structures (bottom). The under layers Al and O atoms of alumina are displayed by white and gray colors, respectively.

adsorbed 2-butanols (Fig. 3, bottom). The larger deviation in energy of adsorbed alcohol is understandable since each rotation about any angle would have a different interaction with the surface. In this study, the focus was on the most stable and the least stable conformers (Fig. 4). Also, the optimized geometries of more stable conformations doped in the alumina nanochannel are shown in Fig. S3. These conformations are utilized in Section 3.5 to shed light on the mode of elimination of 2-butanol over γ-alumina.

The results predict that for staggered conformations of free 2-butanol, the (ap–sc) conformer (where CH_3/CH_3 groups are *anti* and CH_3/OH groups are gauche) is more stable than the (sc–ap) and (sc–sc) conformers. Of the eclipsed conformations, the (ac–ac) conformation is an energy minimum in comparison to the (ac–sp) and (sp–ac) conformations (Fig. 3 and Table 2).

The staggered conformation of the adsorbed (*S*)-2-butanol with (sc–ap) and (sc–sc) rotamer is more stable than the (ap–sc) rotamer. Although, the deviations in the calculated energy values are relatively large for rotamers with dihedral angles of 50–100°. The distribution plot drawn by MATLAB-7.0 program clearly predicts an overwhelming stability of the two former rotamers over the (ap–sc) rotamer. The eclipsed (ac–sp)-conformation of the (*S*)-isomer is less stable than the (ac–ac) and (sp–ac) conformations. This instability is most likely a result of the eclipsed conformation of OH/CH_3 groups and of repulsive interaction of the methyl group

Table 2
Dihedral angle and relative energy of free 2-butanol, adsorbed (*S*)- and (*R*)-2-butanol conformers over γ-alumina (1 0 0) surface.

Conformer	Dihedral angle (°) CH_3–C–C–OH	Dihedral angle (°) CH_3–C–C–CH_3	Relative energy (kcal mol^{-1})
Free 2-butanol			
sc–ap	±172.873	±64.974	0.00
sp–ac	−121.345	0.005	4.51
sc–sc	−62.704	60.483	0.35
ac–sp	−1.521	119.998	4.72
ap–sc	+67.891	−170.404	−0.14
ac–ac	+118.879	−119.999	3.01
Adsorbed (*S*)-2-butanol			
sc–ap	±171.416	±67.833	0.00
sp–ac	−126.780	−5.667	5.04
sc–sc	−65.549	+56.221	0.00
ac–sp	−6.786	+114.908	6.97
ap–sc	+77.765	−162.110	2.52
ac–ac	+124.349	−116.164	5.03
Adsorbed (*R*)-2-butanol			
sc–ap	±168.495	±68.017	0.00
ac–ac	−121.431	+114.121	4.71
ap–sc	−65.919	+170.489	0.22
ac–sp	+6.699	−118.177	8.84
sc–sc	+77.443	−48.782	2.74
sp–ac	+127.205	+2.608	5.26

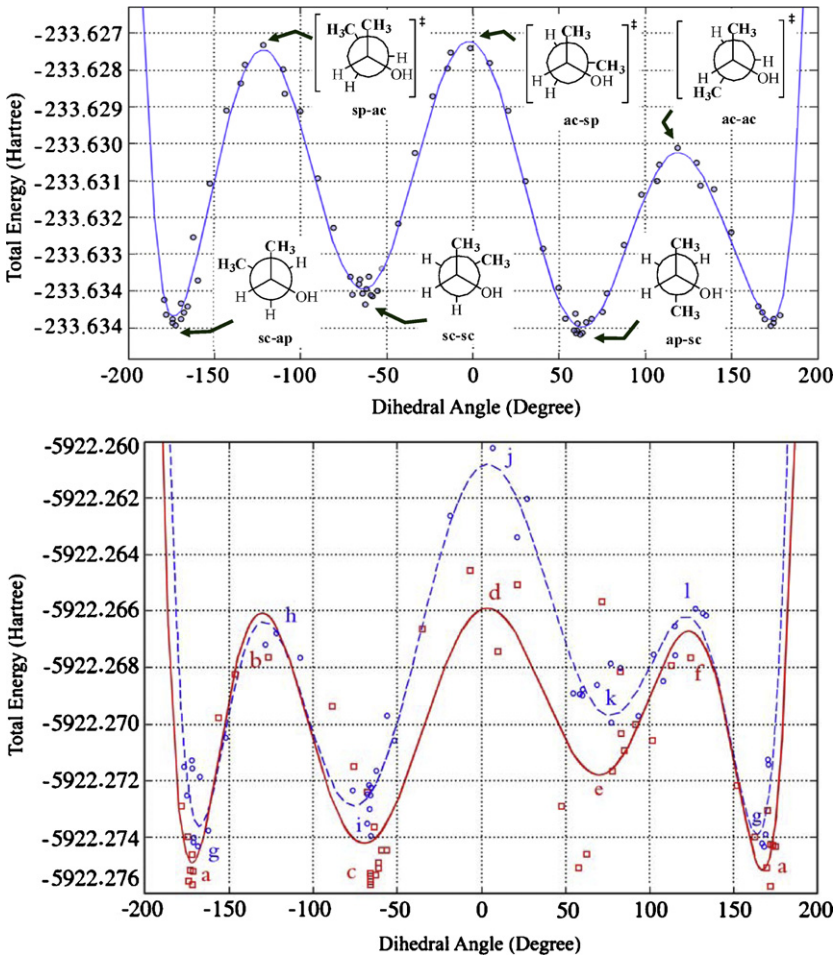

Fig. 3. Potential energy scan diagrams for rotation of free 2-butanol (top) and adsorbed (*S*)-2-butanol (a–f, —) and (*R*)-2-butanol (g-l,---) over γ-alumina (1 0 0) surface (bottom) about CH_3C–COH bond.

on the C3 carbon with the surface of the catalyst (Figs. 3 and 4 and Table 2).

The conformational analysis plot for the adsorbed (*R*)-2-butanol shows that the energies for all (*R*)-rotamers are higher (with much smaller deviation) than those of (*S*)-rotamers. The large variation in energy values for the (*S*)-rotamers could be a result of sensitivity of interactions of these rotamers with respect to the surface. The (*R*)-rotamers are adsorbed at longer distance from surface than the (*S*)-rotamers and therefore their rotation is less sensitive to the surface. These plots clearly demonstrate that (*R*)-2-butanol has a higher energy (as a result of repulsive interaction of the methyl group on C2 with the surface, see Fig. 4) and form a weaker bond with the surface. The plot also shows that the staggered (sc–ap) and (ap–sc) conformations of the (*R*)-isomer are more stable than the (sc–sc) rotamer. This instability is due to two gauche conformations (CH_3/CH_3 and CH_3/OH) and the repulsive interaction of the two methyl groups on C2 and C3 with the surface. The eclipsed conformations (sp–ac) and (ac–ac) are more stable than the (ac–sp) conformation. The energy barrier for interconversion of the two rotamers [(sc–ap)⇆(sc–sc)] of adsorbed (*S*)-2-butanol is 5.0 kcal mol^{-1} which is higher than desorbed alcohol by 0.5 kcal mol^{-1}. The energy barrier for interconversion of the two rotamers [(sc–sc)⇆(ap–sc)] of adsorbed (*S*)-2-butanol and desorbed alcohol are 6.97 and 4.72 kcal mol^{-1}. The energy barrier for interconversion of two rotamers [(sc–ap)⇆(ap–sc)] and [(ap–sc)⇆(sc–sc)] of adsorbed (*R*)-2-butanol are 4.71 and 8.84 kcal mol^{-1} (Table 2). These values indicate that the interaction of the alcohol with the surface increases the energy barrier for rotation.

3.3. Adsorption details

Selected bond lengths, bond angles, and Mulliken atomic charges for the most stable conformers of adsorbed (*R*)- and (*S*)-2-butanol over (1 0 0) γ-alumina surface are listed in Table 1. (*S*)-2-Butanol (sc-ap conformer) is physisorbed on the surface at a distance of 2.05 Å. This distance is longer than that between Al and O atoms of the surface. By changing the central penta-coordinated aluminum atom (Al_c) into a hexa-coordinated aluminum atom, the surface bond lengths changed from 1.881 to 1.952 Å. The OH bond of the 2-butanol molecule formed a staggered conformation with Al–O bonds of the cluster (Fig. 5). The $O_{alcohol}$–Al_c–O_a angle is 92.2°, while the $O_{alcohol}$–Al_c–O_c angle is 86.6° which deviate from 90°. Adsorption of alcohol on the surface is responsible for the deviations in the bond length and bond angle. In the bare (1 0 0) surface external O_a–Al_c–O_c and O_d–Al_c–O_e bond angles are equally 98.6°. These angles for the (1 0 0) surface after adsorption are 98.55 and 98.96°. The internal O_a–Al_c–O_d or O_c–Al_c–O_e angles in the bare surface are 81.6°, which is 1.2° larger than this angle for the adsorbed surface.

The O–H and C–O bond lengths are 0.977, 1.489 Å, respectively. The C–O–H bond angle of adsorbed (*S*)-2-butanol (sc–ap conformer) on the surface is 108.5°. The O–H and C–O bond lengths are 0.977, 1.489 Å, respectively. The C–O–H angle of 2-butanol

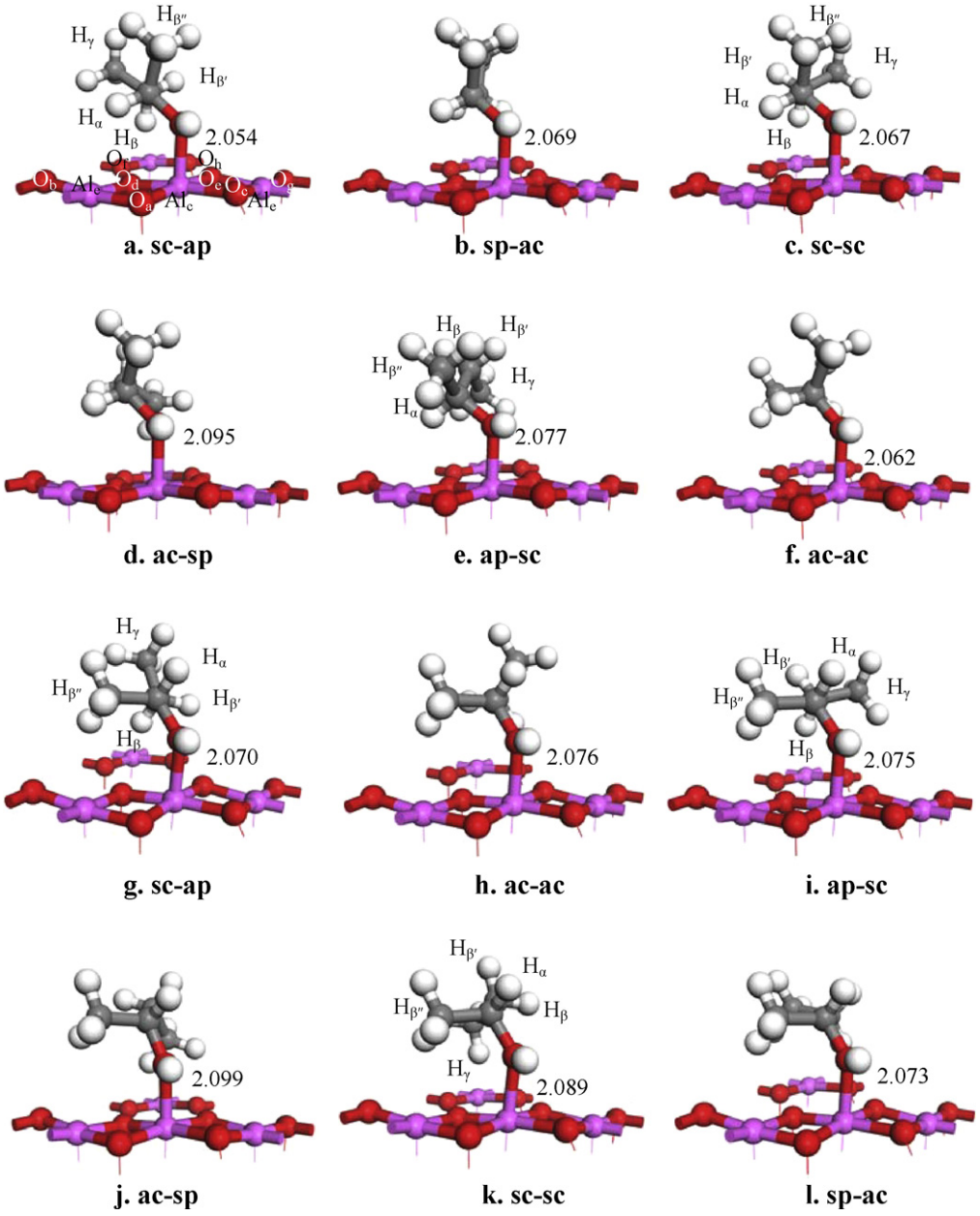

Fig. 4. Selected optimized geometry of conformations of adsorbed (*S*)-2-butanol (a–f) and (*R*)-2-butanol (g–l) over γ-alumina (1 0 0) surface at BLYP/DNP level of theory.

molecule in the gas phase is 108.8°. These values show that adsorption of (*S*)-2-butanol on the surface slightly perturbs the bond length and bond angle of the alcohol (Table 1).

The Al_c–$O_{alcohol}$ bond length for adsorbed (*R*)-2-butanol is 2.07 Å, which is 0.02 Å longer than for adsorbed (*S*)-2-butanol. The C–O–H, C–$O_{alcohol}$–Al_c, H–$O_{alcohol}$–Al_c bond angles for adsorbed *R*-isomer and *S*-isomer are 110, 138, 104° for the former and 108, 127, 102° for the latter. The large increase (11°) in C–$O_{alcohol}$–Al_c bond angle is a result of the position of the methyl group on the chiral C2 carbon atom. The methyl group of the adsorbed *R*-isomer is forced to accept a strained position with the surface. To reduce this repulsion, the bond angle is increased by 11°.

The adsorption energies for (*R*)- and (*S*)-2-butanol are −28.15 and −29.95 kcal mol^{-1}, respectively. The calculated energy for adsorbed (*R*)-2-butanol over the (1 0 0) surface is about 0.8 kcal mol^{-1} (depending on the conformer) less than the adsorbed (*S*)-2-butanol (Table 1). Dissociation energies for (*S*)-2-butanol at different oxygen sites O_a and O_c are −35.14 and −19.12 kcal mol^{-1}. The adsorption and dissociation energies for (*R*)- and (*S*)-2-butanol over the (1 0 0) surface indicate that the (*S*)-isomer forms a stronger bond with the surface than the (*R*)-isomer.

The calculated total density of state (DOS) diagrams for pure alumina (1 0 0) surface and nanochannel are shown in Fig. S4 (a and b). The DOS diagrams indicated three distinct bands. The (2s) O states are found in the left region of diagrams (negative energies). The valence band, which appeared at the center of diagrams (bellow the Fermi level) arises entirely from 2p (O) and (3s) Al atomic orbitals. The conduction band emerged in the right region of diagrams (positive energies). After water adsorption, small bands related to H_2O molecular orbital levels were observed in the DOS diagram (Fig. S4c), which is in agreement with the previous reports in the literature [28,61]. Shapovalov and Truong [61] reported that the band which emerged below the first band of the surface is due to 1s (H) and 2s (O) atomic orbitals or 2a1 level of water. The next band observed below the valence band of surface is due to 1b2 level of water. The 3a1 and 1b1 levels overlapped with alumina valence

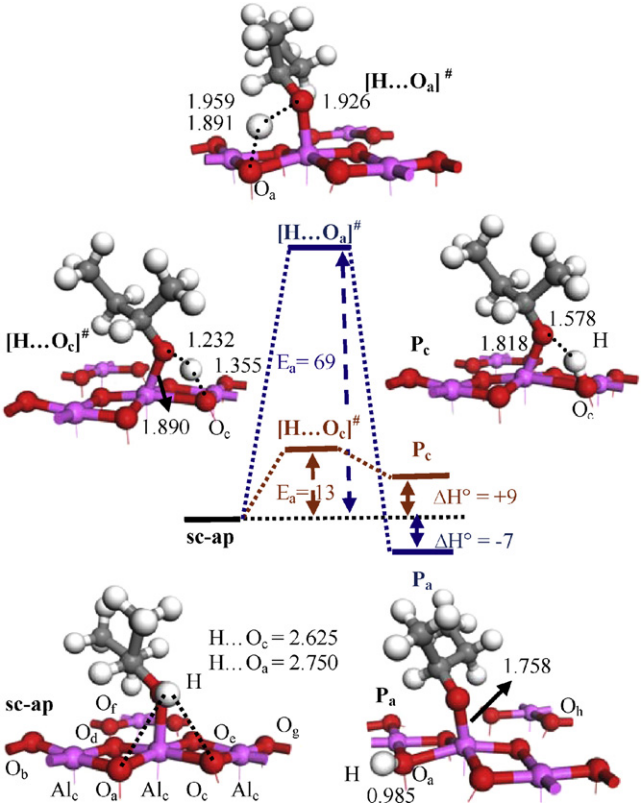

Fig. 5. Adsorption and calculated H-shift mechanism of (*S*)-2-butanol (sc–ap conformer) via oxygens (O_c and O_a) of γ-alumina (1 0 0) surface at BLYP/DNP level of theory (E_a and ΔH° in kcal mol^{-1}).

band [61]. The DOS plots for all adsorbed (*S*) and (R)-2-butanol conformers over alumina (1 0 0) surface and nanochannel are shown in Figs. S5 and S6, respectively. Several atomic orbitals of these conformers were appeared below the valence band and some were mixed with the surface orbitals. As shown in these figures, there is a small difference in the DOS diagrams.

The Mulliken charges distribution of pure γ-alumina (1 0 0) surface, free 2-butanol and adsorbed 2-butanol over the surface are listed in Table 1. In the pure surface, the charge densities for penta-coordinated aluminum sites (Al_c and Al_e), oxygens (O_a, O_d, O_g and O_f) and oxygens (O_e, O_b, O_h, O_c) are 1.385, −0.944 and −0.974. For the adsorbed (*S*)-2-butanol surface, the charge density of Al_c is 1.551 and for Al_e the charge densities are 1.384, 1.399. The charge density for pure hexa-coordinated aluminum is 1.635. This indicates that adsorption of 2-butanol on the surface reduces the charge density of Al_c, but increases the charge density (stronger Lewis acid site) on Al_e adjacent to Al_c. The charge density of Al_e after adsorption of 2-butanol is higher than Al_e of bare surface. This feature was confirmed by the lowest unoccupied molecular orbital (LUMO) electron contours of (1 0 0) surface before and after the adsorption (Fig. S7). Clearly, it was shown that the LUMO electron contour is reinforced on the Al_e site after the adsorption. The oxygen atom of the free 2-butanol has −0.49 negative charge which is slightly more positive than the corresponding value for the adsorbed 2-butanol (−0.56), since the C–$O_{alcohol}$ and H–$O_{alcohol}$ bond lengths of the free alcohol are shorter than the adsorbed molecule. These shorter bonds increase the negative charge of $O_{alcohol}$ (after adsorption) and compensated for the charge transfer between hydroxyl group of alcohol and Al_c site of alumina. In agreement with these results, the charge of hydrogen atom of OH group changes from 0.23 to 0.27 after adsorption.

Mulliken charges for the adsorbed isomers also predict the stability of the (*S*)-isomer over the (*R*)-isomer. The charge densities on the $O_{alcohol}$ and Al_c atoms for the (*S*)-isomer are −0.561 and 1.551 and for the (*R*)-isomer −0.575 and 1.557, respectively. The larger negative charge on $O_{alcohol}$ and positive charge on Al_c for the (*R*)-isomer indicate a weaker interaction with the surface (weaker bond with Al_c). These facts demonstrate that configurationally the (*S*)-isomer forms a stronger bond with the surface than the (*R*)-isomer (Table 1).

3.4. Proton migration of adsorbed 2-butanol

The feasibility of proton migration of adsorbed alcohol [R–O(H)–Al–$O_{(a-h)}$ → R–O–Al–$O_{(a-h)}$H] to adjacent oxygen of the surface was investigated (Scheme 1). Migration of the proton of the (*S*)-isomer (sc–ap conformer) to oxygen O_c is an endothermic process (+9.19 kcal mol^{-1}) with a small activation energy (13.56 kcal mol^{-1}). Migration of the proton to oxygen O_a is an exothermic process (−6.83 kcal mol^{-1}) with a large activation energy (69.34 kcal mol^{-1}) (Table 1, Fig. 5). The proton shift is a kinetically controlled process. The pathway with larger E_a leads to a more stable product (ΔH° = −6.83 kcal mol^{-1}) and the one with smaller E_a is responsible for the formation of a less stable product (ΔH° = +9.19 kcal mol^{-1}). The distance that the proton must migrate to oxygen (O_a or O_c) of the surface controls this process. The distance for migration of the proton to site O_c is shorter than to site O_a. This makes the former proton transfer pathway more feasible. The Al–$O_{alcohol}$, H–O_c bond lengths and H-bonding distance between H and $O_{alcohol}$ [Al–O_c–H···$O_{alcohol}$–R] are 1.818, 1.033 and 1.578 Å, respectively. This makes the H–O_c bond longer than the normal O–H bond. This type of hydrogen bonding was not observed for migration of the proton to O_a. The bond lengths of Al–$O_{alcohol}$ and H–O_a, were 1.758 and 0.985 Å, respectively. The H-shift to site O_c will be much faster than to site O_a (higher E_a). The former is a kinetically controlled process and the latter a thermodynamically controlled process (Fig. 5). The reverse H-shift from site H–O_a to C–$O_{alcohol}$ is very slow due to the high energy of activation. The second factor that makes migration to O_c more favorable is the larger $HO_{alcohol}$–AlO_c dihedral angle. The angles for proton migration to O_c and O_a are 49.80 and 48.60°, respectively. The third factor for the ease of proton migration to site O_c is the higher basic strength of the O_c oxygen. The Mulliken charge on O_c and O_a of sc-ap conformer of (*S*)-2-butanol is −1.000 and −0.977, respectively (Table 1).

3.5. Mechanism of dehydration and dehydrogenation of 2-butanol over γ-alumina (1 0 0) surface and nanochannel

Dehydration studies on secondary alcohols have been found useful in investigating the properties of dehydration catalysts as well as the modes of elimination to yield various alkenes [62–64]. There are reports that alumina is responsible for the formation of ethers [65] and for ketones [66,67]. Competition between these pathways depends on the catalyst morphology, acidity, calcination temperature, reaction temperature, and other factors [64]. Stereochemistry of E2 elimination (*anti* or *syn*) in concerted reactions depends upon substrate and steric interaction of intermediate and transition state. The mode of elimination for the dehydration reaction over a γ-alumina catalyst has been shown to be *anti* from the antiperiplanar conformation with preference to form the cis isomer, when there is the possibility to form geometric isomers [64].

In our recent attempt to have a better understanding of the mechanism of dehydration of secondary and tertiary alcohols over metal oxides, we investigated the transition state of dehydration reaction of DPP over γ-alumina [64]. We further concluded that dehydration of alcohols over metal oxides depends on steric

Table 3
The $O_{alumina}$–$H_{alcohol}$ distance, activation energy (E_a) and enthalpy (ΔH°) for dehydration of adsorbed 2-butanols over γ-alumina (1 0 0) surface.

Entry	Distance (Å)	E_a (kcal mol^{-1}) assumption 1[a]	E_a (kcal mol^{-1}) assumption 2[b]	ΔH° (kcal mol^{-1})	Product
(*S*)-2-Butanol					
sc–ap Conformer					
O_d–H_β	2.492	124.41*	94.76*	8.05	T2B
O_e–H_β	3.138	135.34	123.18	25.65	T2B
O_f–H_β	3.180	137.63	117.27	12.31	T2B
O_h–H_β	3.687	139.66	131.40	42.63	T2B
O_e–$H_{\beta'}$	3.768	140.42*	102.59*	26.89	C2B
sc–sc Conformer					
O_d–H_β	2.687	124.65*	77.24*	10.56	C2B
O_e–H_β	3.199	132.87	117.39	28.16	C2B
O_f–H_β	3.258	129.99	95.37	14.82	C2B
O_h–H_β	3.667	137.34	136.92	45.15	C2B
O_f–$H_{\beta'}$	4.437	123.65*	129.70	14.82	C2B
(*R*)-2-Butanol					
ap–sc Conformer					
O_d–H_β	2.828	120.63*	87.90*	8.03	T2B
O_e–H_β	3.272	125.82	117.31	25.64	T2B
O_f–H_β	3.318	124.72	95.50	12.29	T2B
O_h–H_β	3.671	129.63	130.24	42.62	T2B
O_d–$H_{\beta''}$	2.929	120.29*	79.05*	12.19	1B
O_b–$H_{\beta''}$	2.981	122.52	90.12	47.69	1B
sc–ap Conformer					
O_d–H_β	2.717	137.61	87.88	10.08	C2B
O_e–H_β	3.139	137.33	73.87*	27.69	C2B
O_f–H_β	3.152	140.77	124.62	14.34	C2B
O_h–H_β	3.499	146.44	132.56	44.67	C2B
O_e–$H_{\beta'}$	2.921	146.34	108.02	26.44	T2B
O_d–$H_{\beta''}$	2.801	131.02	110.72	13.00	1B
O_b–$H_{\beta''}$	2.912	129.28	122.07	48.49	1B
O_a–$H_{\beta''}$	3.611	134.61	130.64	12.59	1B

[a] Assumption 1: Alkenes were located between the surface and upper vacuum slab at a distance of 4.5 Å. Geometry of the main transition states marked by asterisk (*) is shown in Fig. S8(a–f).
[b] Assumption 2: Alkenes were located in the location of the alcohol starting material and these structures were optimized. Geometry of the main transition states marked by asterisk (*) is shown in Fig. 7(a–g).

interaction of intermediate and/or transition state, on the localized adsorption of the reacting molecule on the surface, and its steric restrictions in the transition state. The major disappointment of this work was the non-conclusive computational analysis of the dehydration of 2-butanol. In this case, we did not obtain a transition-state model (similar to that obtained for DPP) to address the mode of elimination for secondary alcohols [64].

Cis-2-butene (C2B), trans-2-butene (T2B) and 1-butene (1B) could be formed by dehydration of 2-butanol over alumina. The optimized geometry of 2-butanol conformers (Figs. 3 and 4) predicts that two conformers (sc-sc) and (ap-sc) are not involved in the elimination reaction of (*R*)- and (*S*)-2-butanol, respectively. Both conformers have a strong repulsive interaction of the methyl group with the surface and neither of the β-hydrogens can interact with the surface. These conformers become important when doped into an alumina nanochannel (Fig. S3).

The distance between basic sites of alumina and β, β′, β″ hydrogens (AlO_{a-h}–$H_{\beta,\beta',\beta''}$), activation energy (E_a), and enthalpy (ΔH°) of the most stable conformers of adsorbed (*R*)- and (*S*)-2-butanol over the (1 0 0) surface were calculated to help shed light on the elimination reaction pathway (starting material (2-butanols/γ-alumina) → transition state $[TS]^\ddagger$ → products) of a secondary alcohol over each basic site (O_{a-h}) of the (1 0 0) surface (Table 3). All basic oxygen sites of the surface at distances less than 4 Å (with the exception of one case AlO_f–$H_{\beta'}$, 4.437 Å) from β, β′ and β″ hydrogens were considered as a site for elimination and were included in our study.

The optimized geometry of catalyst surface after dehydration via basic sites ($O_{a,b,d,e,f,h}$) is presented in Fig. 6. The distances of sites O_c and O_g with β-hydrogens were out of range in the elimination reaction and were excluded from our results. The optimized geometry of the (1 0 0) alumina surface predicts stabilization of sites O_a and O_d after dehydration (Table 4). This is why these sites favor elimination of β-hydrogens to produce alkenes. Sites O_b and O_h have the highest energies (least stable). These sites are connected to tetrahedral Al. This change in oxygen coordination number (change of hybridization) increases the bond length between tetrahedral-Al and oxygens, which lowers the stability. The site O_e which is also connected to a tetrahedral Al is more stable than sites O_b and O_h. This stability is a result of hydrogen bonding (1.708 Å) between two adjacent OH groups (Fig. 6). The bond lengths for Al_c–OH and $O_{b,h}$–H are about 1.77 and 0.98 Å and for Al_c–OH and O_e–H are 1.806 and 1.018 Å, respectively. This increase in bond length is a result of the deformation of the OH group to one side to enforce a hydrogen bond with a length of 1.708 Å. However, sites O_a–H, O_d–H, and O_f–H behave differently. The O_a–H and O_d–H sites are located adjacent to site Al_c–OH. Bond lengths of O_a–H, O_d–H and Al_c–OH are 0.985, 0.983 and ≈1.76 Å, respectively. The sites O_f–H and O_d–H are located at distances (form weak hydrogen bonding) of 2.187

Table 4
Relative energy for optimized geometry of γ-alumina (1 0 0) surface after dehydration via O_{a-h} sites that are shown in Fig. 6.

Sites	Relative energy (kcal mol^{-1})
O_a	0.0
O_b	35.9
O_c	17.3
O_d	0.4
O_e	18.0
O_f	4.7
O_g	7.3
O_h	34.99

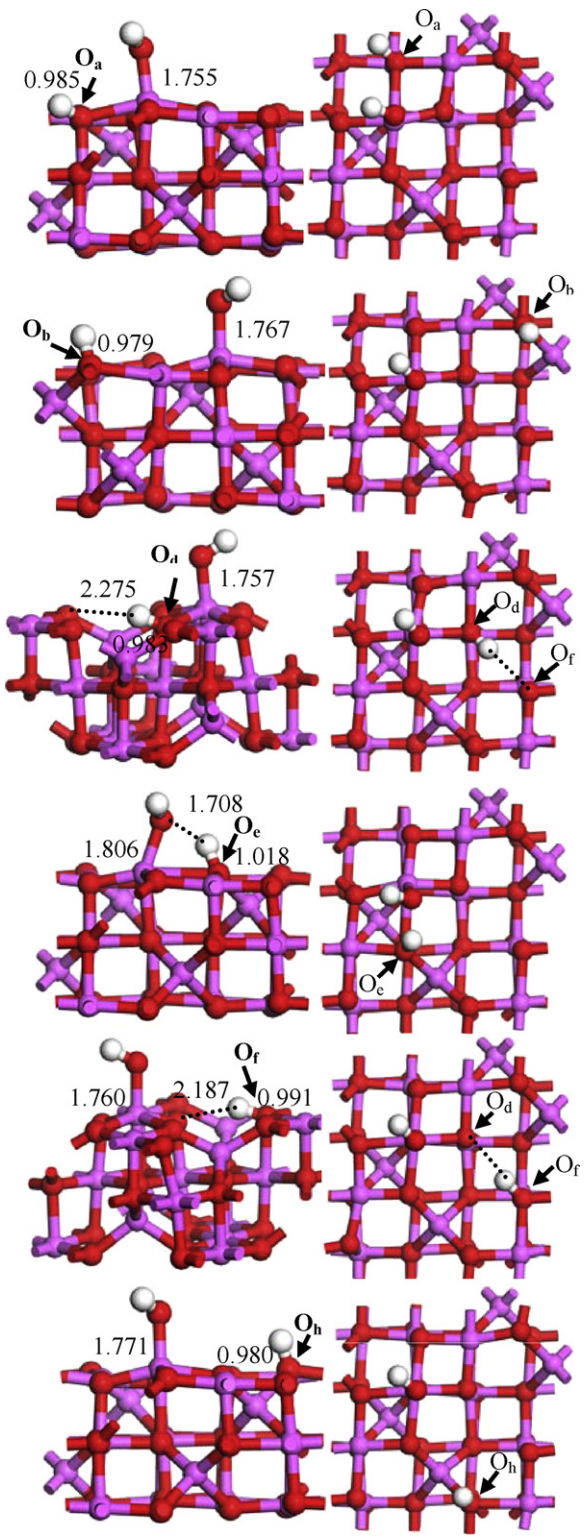

Fig. 6. Optimized geometry of γ-alumina (1 0 0) surface after dehydration of 2-butanol by basic sites O_{a-h} calculated at BLYP/DNP level of theory. Side view (right) and top view (left).

and 2.275 Å for sites O_d and O_f, respectively. The O_a–H site forms a hydrogen bond with the oxygen of next unit cell (Fig. 6). The stability of the catalyst surface of the O_g and O_c sites plays a similar role as for sites O_f and O_e, respectively (Table 4).

The following assumptions were made for the calculation of activation energies: First, there is no interaction between catalyst surface and alkenes when elimination process is completed. The transition state for the elimination pathway was calculated by placing the alkenes over the upper half of the vacuum slab at a distance of 4.5 Å from the surface. At this distance, minimum interaction is assumed between surface and alkenes. The calculated activation energies were quite high (120–150 kcal mol^{-1}) with respect to the AlO_{a-h}–$H_{\beta,\beta',\beta''}$ distances (geometry of the main transition states marked by asterisk (*) in Table 3 is shown in Fig. S8(a–f)). Second, alkenes were placed exactly at the same location (similar coordinates) of the starting material (alcohol) then the structures were relaxed. When the geometry optimization was completed, the alkenes were desorbed from the surface at the distance of 2.5–3.5 Å (smaller than the distance used in assumption 1). The calculated activation energies varied in a range of 70–140 kcal mol^{-1} with respect to the AlO_{a-h}–$H_{\beta,\beta',\beta''}$ distances (geometry of the main transition states marked by asterisk (*) in Table 3 is shown in Fig. 7(a–g)). Third, to find the minimum value of E_a, the calculations were performed using the unrelaxed geometries where alkenes were placed exactly at the same location (similar coordinates) of the starting material (alcohol) using unrelaxed geometries. These calculations were carried out only for the structures with minimum activation energy (47–65 kcal mol^{-1}). The geometry of the main transition states is shown in Fig. 7(i–k). These results indicated that the calculated E_a value is very sensitive to the AlO_{a-h}–$H_{\beta,\beta',\beta''}$ and the distance between alkenes and alumina surface.

The correlation between activation energy and distance of basic sites and β eliminable hydrogens is shown in Fig. 8. The activation energy for elimination of a β-hydrogen from the (*R*)- and (*S*)-2-butanol conformers increases with increasing distance between β-hydrogen and basic site (O_{a-h}) (Table 3, Fig. 8). The best sites for elimination of β-hydrogen from the (*S*)-2-butanol (sc–ap) conformer are O_d, O_e, O_f and O_h, with distances of 2.492, 3.138, 3.180 and 3.687 Å, respectively. The order of reactivity for sites O_e and O_f are reversed for the (ap–sc) conformer of the (*R*)- and (sc–sc) conformer of (*S*)-2-butanol (Table 3). This difference in reactivity depends on the direction of the methyl group. For conformer (sc–ap) of (*S*)-2-butanol, the methyl group faces site O_f and for the (sc–sc) rotamer the methyl group faces site O_e (Fig. 4). Moreover, the O_f site is located at a better situation than O_e for the elimination of β-hydrogen. The same effect is observed for the two conformers (ap–sc) and (sc-ap) of (*R*)-2-butanol. These exceptions are not shown in Fig. 8. The correlation between activation energies and AlO_{a-h}–H_β distances in assumption 2 (Fig. 8, dotted line) are similar to that of assumption 1 (Fig. 8, solid line). The activation energies (using assumption 2) were decreased drastically at shorter distances.

The charge density of the basic site plays a major role in elimination reactions. Mulliken atomic charges on sites O_d, O_e, O_f and O_h for the adsorbed conformer (sc–ap) of (*S*)-2-butanol are −0.976, −0.998, −0.947 and −0.984, respectively. Mulliken charges predict sites O_e and O_h to be the best sites for elimination. However, combination of steric hindrance, distance of β-hydrogen and charge density of the site select the most favorable path for elimination. This confirms our earlier prediction that dehydration of alcohols over metal oxides depends not only on the steric interaction of the intermediate and/or transition state, but is also strongly dependent on the preparation conditions of catalyst and on reaction conditions [64]. Each of these factors has a pronounced effect on the distance of the eliminable hydrogen and the charge density of the site.

E2 elimination of β- and β′-hydrogens from the (sc-ap) conformer of (*S*)-2-butanol with synclinal transition state (eliminable $H_{\beta,\beta'}$ and OH leaving group have gauche conformation) leads to trans (Fig. 7a) and cis (Fig. 7b) products, respectively. The activation energy for elimination to give T2B and C2B is 94.76 and 102.59 kcal mol^{-1}, respectively (Table 3, assumption 2). The repulsion between the two methyl groups in the gauche conformation

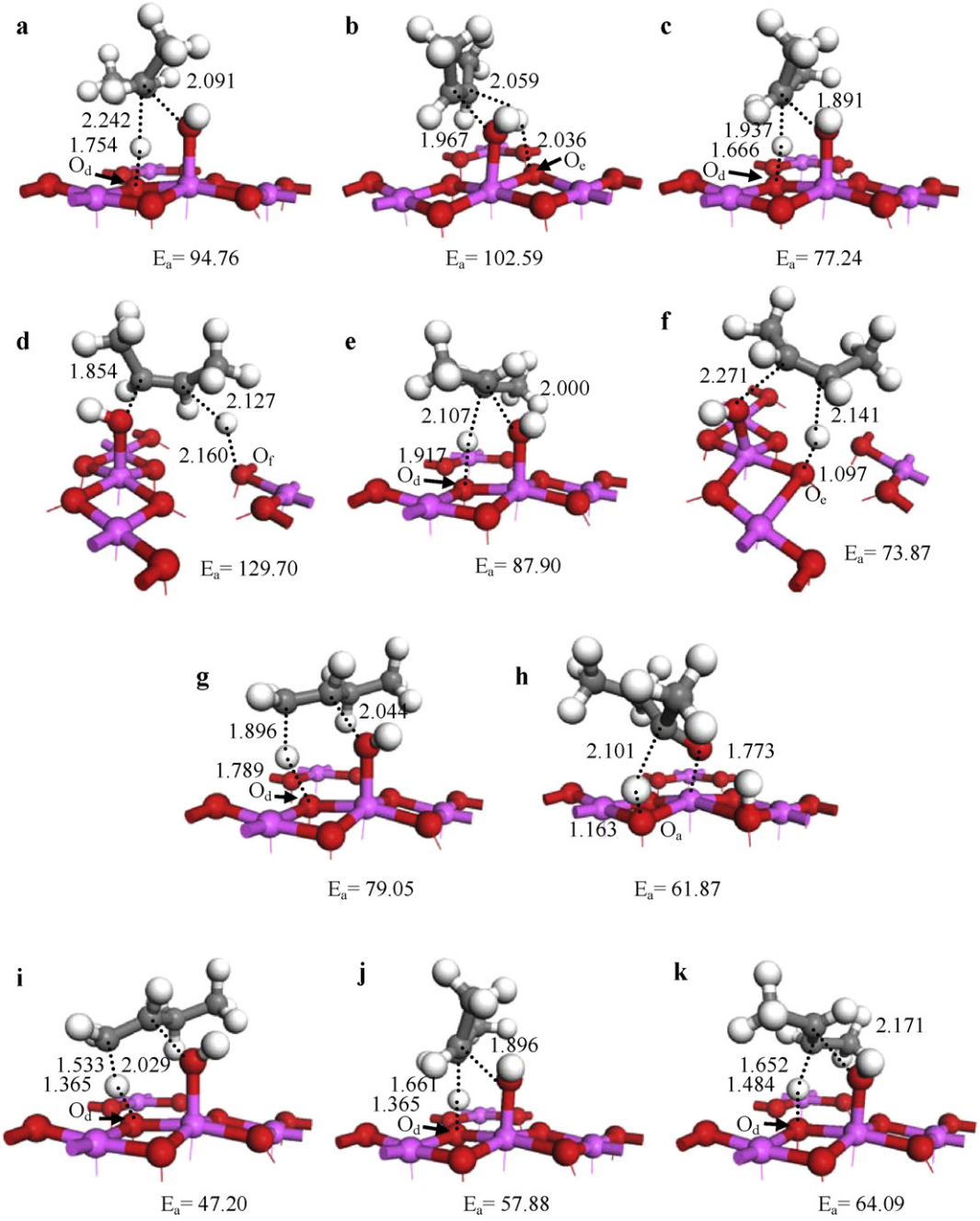

Fig. 7. Calculated transition states for elimination reactions of 2-butanol over γ-alumina (1 0 0) surface based on the assumption 2 (relaxed geometries where alkenes or ketone were located in the location of the alcohol starting material and these structures were optimized, a–h) and assumption 3 (unrelaxed geometries where alkenes were fixed in the location of the alcohol starting material, i–k). (a and b) E2 synclinal dehydration of (sc–ap) conformer of (*S*)-2-butanol to form trans and cis-2-butene, respectively. (c and d) E2 synclinal and antiperiplanar dehydration of (sc–sc) conformer of (*S*)-2-butanol to from cis-2-butene, respectively. (e) E2 synclinal dehydration of (ap–sc) conformer of (*R*)-2-butanol to form trans-2-butene. (f) E2 synclinal dehydration of (sc–ap) conformer of (*R*)-2-butanol to from cis-2-butene. (g) E2 synclinal dehydration of (ap–sc) conformer of (*R*)-2-butanol to form 1-butene. (h) Dehydrogenation transition state model of (sc–ap) conformer of (*S*)-2-butanol. (i) Similar to (g) for assumption 3. (j) Similar to (c) for assumption 3. (k) Similar to (e) for assumption 3. E_a is in kcal mol^{-1}.

increases the energy for the formation of the cis isomer. The distances between O_d–H_β (2.492 Å) and O_e–$H_{\beta'}$ (3.768 Å) also contributes to the higher energy barrier for the formation of the cis isomer with synclinal transition state. The (sc–sc) conformer of (*S*)-2-butanol (activation energy 77.24 kcal mol^{-1}) eliminates H_β via O_d with synclinal transition state (Fig. 7c) to form C2B (Table 3, assumption 2). This value is smaller than E_a of the (sc–ap) conformer because the distance between O_d and H_β (2.687 Å) is smaller than that between O_e and $H_{\beta'}$ (3.768 Å). E2 elimination of $H_{\beta'}$ via site O_f from the (sc–sc) conformer with an antiperiplanar transition state ($H_{\beta'}$ and OH leaving group have anti conformation) produces C2B with lower activation energy (129.70 kcal mol^{-1}) than expected value, despite having a longer distance (4.437 Å), Fig. 7d, Table 3, assumption 2. E2 elimination of H_β via O_d from the (ap–sc) conformer of (*R*)-2-butanol with activation energy of 87.90 kcal mol^{-1} produces T2B (Fig. 7e, Table 3, assumption 2). This value is smaller than the E_a of (sc–ap)-(*S*)-2-butanol, due to a decreased repulsion of the methyl groups in the transition state. E2 elimination of H_β from (sc–ap) conformer of (*R*)-2-butanol with synclinal transition state (activation energy of 73.87 kcal mol^{-1})

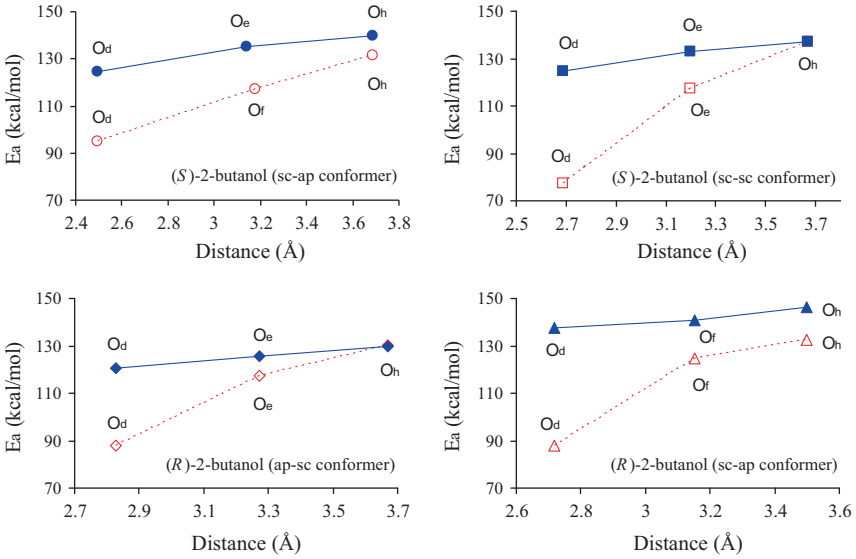

Fig. 8. Correlation between activation energy and distance of $O_{alumina}$–$H_{\beta\ alcohol}$ for (*S*)- and (*R*)-2-butanol conformers calculated based on assumption 1 (alkenes were located between the surface and upper vacuum slab at a distance of 4.5 Å, solid line) and assumption 2 (alkenes were located in the location of the alcohol starting material and these structures were optimized, dotted line). The corresponding $O_{alumina}$ site of activation energies is shown on figures.

produces C2B (Fig. 7f, Table 3, assumption 2). 1B produces from the E2elimination of $H_{\beta''}$ of (ap–sc)-(*R*)-2-butanol via site O_d with activation energy of 79.05 kcal mol^{-1} (Fig. 7g, Table 3, assumption 2).

The computed transition state for the dehydrogenation of the (sc–ap) conformer of (*S*)-2-butanol is shown in Fig. 7h. In this model, adsorbed alcohol over the catalyst (1 0 0) surface with H-shift to site O_c is used to compute the dehydrogenation pathway (Fig. 5). We noted earlier (Section 3.4) that migration of hydrogen of adsorbed alcohol to site O_c produces an unstable surface with small activation energy (13.56 kcal mol^{-1}). This unstable surface has the potential to eliminate α-hydrogen (with activation energy of 61.87 kcal mol^{-1}) and simultaneously lose the adsorbed alkoxy from the surface to produce 2-butanone. The distance of the basic site of the surface (O_a) and α-hydrogen is 2.889 Å which is in good range for elimination.

In the following, we considered the anti elimination of (*R*)- and (*S*)-2-butanol conformers doped into a (1 0 0) alumina nanochannel. This investigation was constructed based on Pines and Pillai transition state model [68], which assumes that two layers of alumina that acidic and basic centers are located on opposite walls are involved in anti elimination of 2-butanol (Fig. S3). The distance of basic site (O_{a-h}) of top layer and $H_{\beta,\beta',\beta''}$ of adsorbed alcohol, activation energies (E_a), and enthalpies (ΔH°) are listed in Table 5. The

Table 5
The $O_{alumina}$–$H_{alcohol}$ distance, activation energy (E_a) and enthalpy (ΔH°) for dehydration of adsorbed 2-butanols over γ-alumina (1 0 0) nanochannel.

Entry	Distance (Å)	E_a (kcal mol^{-1}) [a]	ΔH° (kcal mol^{-1})	Product
(*S*)-2-Butanol				
sc–ap Conformer				
O_f–$H_{\beta''}$	3.221	81.99*	50.74	1B
O_d–$H_{\beta''}$	3.203	88.52	50.51	1B
sc–sc Conformer				
O_f–$H_{\beta''}$	3.157	82.19	53.33	1B
O_d–$H_{\beta''}$	3.192	86.58	50.37	1B
O_d–$H_{\beta'}$	4.128	116.62	56.02	C2B
ap–sc Conformer				
O_d–H_{β}	3.088	86.64*	63.34	T2B
O_e–$H_{\beta'}$	3.310	123.96	76.51	T2B
O_f–$H_{\beta''}$	3.511	85.34	53.82	1B
(*R*)-2-Butanol				
ap–sc Conformer				
O_d–$H_{\beta'}$	3.926	103.75	54.37	T2B
O_b–$H_{\beta''}$	4.204	110.32	77.24	1B
sc–ap Conformer				
O_b–$H_{\beta''}$	4.235	127.42	89.11	1B
sc–sc Conformer				
O_d–$H_{\beta'}$	3.248	99.24	53.89	C2B
O_e–$H_{\beta'}$	3.676	84.32*	68.38	C2B
O_b–$H_{\beta''}$	4.250	113.26	74.07	1B

[a] Geometry of the main transition states marked by asterisk (*) is shown in Fig. 9(a–c).

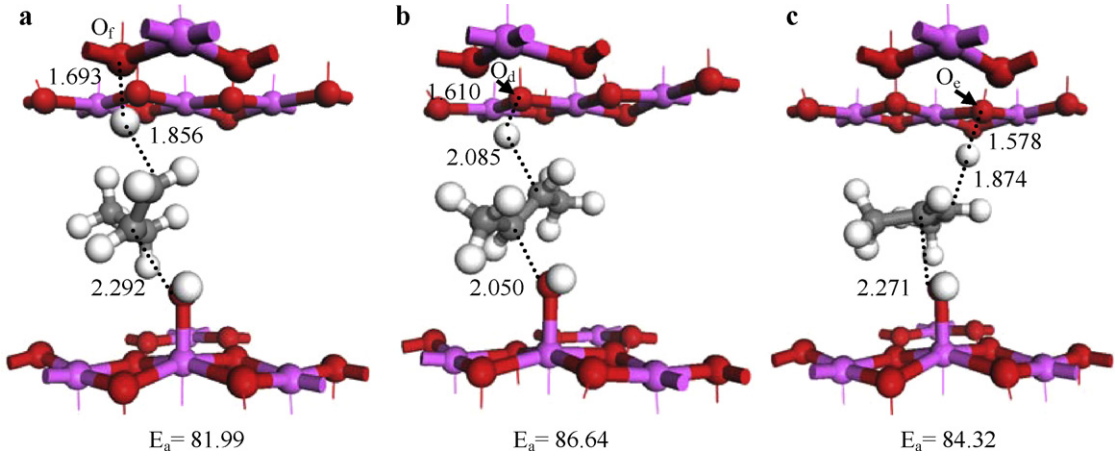

Fig. 9. Calculated transition states for E2 antiperiplanar dehydration of 2-butanol over γ-alumina (1 0 0) nanochannel: (a) Dehydration of (sc–ap) conformer of (*S*)-2-butanol to form 1-butene. (b) Dehydration of (ap–sc) conformer of (*S*)-2-butanol to form trans-2-butene. (c) Dehydration of (sc–sc) conformer of (*R*)-2-butanol to form cis-2-butene.

calculated activation energies vary in a range of 80–130 kcal mol^{-1} with respect to the AlO_{a-h}–$H_{\beta,\beta',\beta''}$ distances. Geometry of the main transition states marked by asterisk (*) in Table 5 are shown in Fig. 9(a–c). The minimum value of E_a is related to formation of 1B from (sc–ap) conformer of (*S*)-2-butanol (81.99 kcal mol^{-1}, Fig. 9a). The activation energy for the formation of T2B and C2B from (ap–sc)-(*S*)-2-butanol and (sc–sc)-(*R*)-2-butanol is 86.64 and 84.32 kcal mol^{-1}, respectively (Fig. 9b and c).

Comparison of the activation energy values (based on assumption 2) of 2-butanol dehydration (Fig. 7a–g) with that of dehydrogenation (Fig. 7h) predicts that E_a for 2-butanone pathway is smaller than that of alkenes; therefore, the ketone is formed predominantly at lower reaction temperature. At higher temperature the activation energy is provided for the formation of alkenes. This feather was observed experimentally by Shi and Davis [65]. According to the results (based on assumption 2) the following activation energy sequence of alkenes is obtained C2B < 1B < T2B. These results predicted that the energy barrier for C2B pathway is about 5 and 14 kcal mol^{-1} smaller than 1B and T2B, respectively. This is in accord with the experimental findings at initial time on stream (Fig. S9).

When, the calculations were performed for the unrelaxed geometries (assumption 3) the activation energies was decreased (47.20 kcal mol^{-1} for1B, 57.88 kcal mol^{-1} for C2B and 64.09 kcal mol^{-1} for T2B) and the energy sequence was changed to 1B < C2B < T2B (Fig. 7i–k). This sequence is in agreement with the calculated values for the nanochannel model (1B < C2B < T2B). These results indicate that the required energy barrier for the formation of 1B is almost 10 kcal mol^{-1} smaller than C2B. The activation energy for T2B pathway is approximately 6 kcal mol^{-1} higher than that of C2B (Fig. 7i–k).

The comparison of calculated activation energies over dehydroxylated (1 0 0) γ-alumina surface with other alumina species such as amorphous alumina or (1 1 0) surface of γ-alumina is difficult because of the complex nature of alumina surface. For instance, the upper layer of (1 0 0) surface is formed by penta-coordinated aluminum and tri-coordinated oxygen atoms while, the (1 1 0) surface has both tri- and tetra-coordinate aluminum and tri-coordinated oxygen atoms. The tri-coordinated aluminum atoms are stronger Lewis acids than penta-coordinated [50]. In the case of amorphous alumina the coordination number of Al and O atoms varies in a range of 4–6 and 2–4, respectively [69]. Therefore, a future work on the hydroxylated and dehydroxylated (1 0 0) and (1 1 0) γ-alumina surfaces should shed some light to this comparison. The elimination reactions of (*R*)- and (*S*)-2-butanol over these surfaces are now under way at DFT level of theory.

3.6. Experimental versus theoretical

There have been a number of attempts to compare the mechanisms of the reactions of alcohols (experimentally) over alumina [65,70,71]; many discrepancies, however, have resulted under different reaction conditions and/or reagents used for the preparation of the catalyst. Another difficulty is secondary reactions (isomerization, dehydrogenation, and ether formation) over the catalyst surface. The catalysts are modified (by blocking acid or basic sites using adsorbed species), alcohols are diluted in other mediums (inert gases, non-reactive solvents or alcohols with higher number of carbons) and the temperature is lowered or the liquid hourly space velocity (LHSV) is increased in order to prevent these reactions. All these actions could have an adverse effect on the mechanism of dehydration.

In this work, the reactivity and selectivity of 2-butanol over γ-alumina (catalyst preparation and reaction conditions are described in supporting information) was monitored in the gas phase under different alcohol conversions (at various temperatures and LHSV) in one run (this minimizes the errors reported by different research group [70]) using the same catalyst (Fig. S9). This figure predicted that reactivity and product distribution are very sensitive under different reaction conditions.

Correct comparison of the experimental values with theoretical findings requires appropriate measures. First, the use of correct model to compute the catalyst surface with or without the adsorbed species. Second, the use of appropriate experimental conditions which are comparable with the theoretical gas phase calculation. Third, the use of experimental condition which does not alter the mechanism but at the same time prevents secondary isomerization. Furthermore, the elimination of a water molecule from such a transition state is certainly influenced by inductive effects, alkene stabilizing effects (hyperconjugation), statistical effects (number of β-hydrogens available for elimination), and steric effects. Finally, other experimental features such as the interaction between adsorbates, coverage effects and polymerization must be considered. These factors play a major role experimentally; however, most theoretical models do not include them in calculations.

We believe catalyst surface exhibits several types of reactive site each exhibiting different reactivity and/or selectivity due to the asymmetric nature of each site. The reactivity and selectivity

of these sites are directly related to the reactant, reaction conditions, time on stream and the environment of each site. The most active sites (fewer in number) produce the less selective product distribution at a faster rate (first several hours, time on stream). The sites with moderate activity (large in number) give products with high stereo and regieoselectivity. The sites with lowest activity (slower rate of conversion, may or may not give rise to selective adducts) require harsher condition to convert reactant to less selective products (near at thermodynamic equilibrium composition).

The above discussions may justify the conclusion that, exact comparison between experimental and theoretical findings is impossible. However, the computations which were carried out in this work clearly but qualitatively complemented the experimental findings.

4. Conclusions

The asymmetric property of γ-alumina (1 0 0) surface (defect spinel structure) stems from unsymmetrical holes and vacancies of the bulk alumina. This feature must be responsible for the different adsorption rate of (*R*)- and (S)-2-butanol on the surface. The computed conformational analysis indicates that the energies of all adsorbed (*R*)-2-butanol rotamers are higher than those of (*S*)-rotamers. The (*S*)-isomer forms a stronger bond with the surface than the (*R*)-isomer.

The transition state model for the E2 dehydration reaction over the γ-alumina (1 0 0) surface predicts that the orientation of the adsorbed alcohol and the free rotation about sigma bonds create conformeric structures which can play a major role in the elimination reaction. The steric interaction between adsorbed alcohol and the catalyst surface appears to be more important than intramolecular steric constraints present in the required conformation for elimination. The Mulliken atomic charges predict that selected basic sites (O_{a-h}) play a major role in elimination reactions. E2 elimination with a synclinal transition state is comparable with an E2 antiperiplanar transition state. The activation energy for elimination of β-hydrogen from the (*R*)- and (*S*)-2-butanol conformers increases with increasing distance between β-hydrogen and basic sites.

Three assumptions were made for the calculation of activation energies over the γ-alumina (1 0 0) surface. Based on the assumption 1, alkenes were located between the surface and upper vacuum slab at a distance of 4.5 Å. The calculated activation energies were quite high (120–150 kcal mol^{-1}). Based on assumption 2, alkenes or ketone were placed exactly at the same location (similar coordinates) of the starting material (alcohol) and then their geometries were optimized. The calculated activation energies varied in the range of 70–140 kcal mol^{-1}. These results predicted the energy barrier for C2B pathway is about 5 and 14 kcal mol^{-1} smaller than for 1B and T2B, respectively (this is in accord with the experimental finding). Based on assumption 3, alkenes were placed exactly at the same location (similar coordinates) of the starting material (alcohol) using unrelaxed geometries. In this case, activation energies were decreased to 47–65 kcal mol^{-1}. The energy barrier for 1B pathway is 10 kcal mol^{-1} smaller than for C2B pathway. The activation energy for T2B pathway is approximately 6 kcal mol^{-1} higher than that of C2B. These results indicated that moreover the AlO_{a-h}–$H_{\beta,\beta',\beta''}$ distances, the calculated value of E_a is also very sensitive to the distance between alkenes and alumina surface.

The distance between the layers of (1 0 0) alumina nanochannel must be at least 8 Å for the doped 2-butanol to achieve the minimum energy. The calculated activation energies when acidic and basic centers were located on the opposite walls of nanochannel were varied in the range of 80–130 kcal mol^{-1}.

The calculations show that the significant similarities and differences for the conversion of the (*R*)- and (*S*)-2butanols are:

1. The activation energy for E2elimination of H_β via O_d from the conformer (ap–sc)-(*R*)-2-butanol is smaller than that of (sc–ap)-(*S*)-2-butanol, due to a decreased interaction of the methyl groups in the transition state.
2. The best site for elimination of β-hydrogen from the (sc–ap) and (sc–sc) conformers of (*S*)-2-butanol and (ap–sc)-(*R*)-2-butanol is O_d, while for (sc–ap)-(*R*)-2-butanol is O_e.
3. The order of reactivity for sites O_e and O_f are reversed for all conformers of the (*R*)- and (*S*)-2-butanol.
4. C2B and T2B were produced by E2 elimination of H_β and $H_{\beta'}$ of conformer (sc–ap)-(*R*)- and (*S*)-2-butanol.
5. E2 elimination of $H_{\beta''}$ of ap–sc and sc–ap conformers of (*R*)-2-butanol produces 1B.

In addition, the dehydroxylated model alumina surface was used for this report (since experimentally most of hydroxyl moiety is lost at high calcination temperature). Experimentally, reactivity and product distribution of 2-butanol over γ-alumina was found to be very sensitive under different reaction conditions. This makes a reliable quantitative comparison between experimental and theoretical values difficult. However, the qualitative theoretical findings complement the E2 elimination mechanism. Experimental reaction of (*R*)- and (*S*)-2-butanol over γ-alumina is now underway.

Acknowledgements

We would like to thank the Isfahan University of Technology (IUT) research council for financial support (Grant # 88/500/9143).

Appendix A. Supplementary data

Supplementary data associated with this article can be found, in the online version, at doi:10.1016/j.molcata.2010.09.016.

References

[1] Y.K. Park, E.H. Tadd, M. Zubris, R. Tannenbaum, Mater. Res. Bull. 40 (2005) 1506–1512.
[2] H.A. Dabbagh, M. Zamani, H. Farrokhpour, M. Namazian, H. Etedali Habibabadi, Chem. Phys. Lett. 485 (2010) 176–182.
[3] L. Pu, X. Bao, J. Zou, D. Feng, Angew. Chem. Int. Ed. 40 (2001) 1490–1493.
[4] D.Y. Geng, Z.D. Zhang, W.S. Zhang, P.Z. Si, X.G. Zhao, W. Liu, K.Y. Hu, Z.X. Jin, X.P. Song, Scripta Mater. 48 (2003) 593–598.
[5] J. Zhou, S.Z. Deng, J. Chen, J.C. She, N.S. Xu, Chem. Phys. Lett. 365 (2002) 505–508.
[6] M. Ma, Y. Zhu, Z. Xu, Mater. Lett. 61 (2006) 1812–1815.
[7] H. Masuda, H. Yamada, M. Satoh, H. Asoh, M. Nakao, T. Tamamura, Appl. Phys. Lett. 71 (1997) 2770–2772.
[8] L. Wilcox, G. Burnside, B. Kiranga, R. Shekhawat, M.K. Mazumder, R.M. Hawk, D.A. Lindquist, S.D. Burton, Chem. Mater. 15 (2003) 51–56.
[9] K.C. Popat, G. Mor, C.A. Grimes, T.A. Desai, Langmuir 20 (2004) 8035–8041.
[10] P. Souza Santos, H. Souza Santos, S.P. Toledo, Mater. Res. 3 (2000) 104–112.
[11] C. Wolverton, K.C. Hass, Phys. Rev. B 63 (2000), 024102-1-16.
[12] P. Rayboud, M. Digne, R. Iftimie, W. Wellens, P. Euzen, H. Toulhoat, J. Catal. 201 (2001) 236–246.
[13] X. Krokidis, P. Rayboud, A.E. Gobichon, B. Rebours, P. Euzen, H. Toulhoat, J. Phys. Chem. B 105 (2001) 5121–5130.
[14] M. Digne, P. Sautet, P. Rayboud, H. Toulhoat, E. Artacho, J. Phys. Chem. B 106 (2002) 5155–5162.
[15] O. Maresca, A. Allouche, J.P. Aycard, M. Rajzmann, S. Clemendot, F. Hutschka, J. Mol. Struct.-Theochem 505 (2000) 81–94.
[16] P. Hirva, T.A. Pakkanen, Surf. Sci. 277 (1992) 389–394.
[17] M. Lindblad, T.A. Pakkanen, Surf. Sci. 286 (1993) 333–345.
[18] J. Fernandez Sanz, H. Rabaa, F.M. Poveda, A.M. Marquez, C. Calzado, J. Int. J. Quantum Chem. 70 (1998) 359–365.
[19] S. Cai, K. Sohlberg, J. Mol. Catal. A: Chem. 248 (2006) 76–83.
[20] S. Cai, V. Chihaia, K. Sohlberg, J. Mol. Catal. A: Chem. 275 (2007) 63–71.
[21] K. Sohlberg, S.J. Pennycook, S.T. Pantelides, J. Am. Chem. Soc. 121 (1999) 7493–7499.
[22] S. Cai, M. Caldararu, V. Chihaia, C. Munteanu, C. Hornoiu, K. Sohlberg, J. Phys. Chem. C 111 (2007) 5506–5513.
[23] M.L. Ferreira, E.H. Rueda, J. Mol. Catal. A: Chem. 178 (2002) 147–160.

[24] D.A. De Vito, F. Gilardoni, L. Kiwi-Minsker, P.Y. Morgantini, S. Porchet, A. Renken, J. Weber, J. Mol. Struct.-Theochem 469 (1999) 7–14.
[25] J. Handzlik, J. Ogonowski, R. Tokarz-Sobieraj, Catal. Today 101 (2005) 163–173.
[26] J. Handzlik, P. Sautet, J. Catal. 256 (2008) 1–14.
[27] A. Vijay, G. Mills, H. Metiu, J. Chem. Phys. 117 (2002) 4509–4516.
[28] A. Ionescu, A. Allouche, J.P. Aycard, M. Rajzmann, F. Hutschka, J. Phys. Chem. B 106 (2002) 9359–9366.
[29] O. Maresca, A. Ionescu, A. Allouche, J.P. Aycard, M. Rajzmann, F. Hutschka, J. Mol. Struct.-Theochem 620 (2003) 119–128.
[30] A. Ionescu, A. Allouche, J.P. Aycard, M. Rajzmann, R.L. Gall, J. Phys. Chem. B 107 (2003) 8490–8497.
[31] F.H. Streitz, J.W. Mintmire, Phys. Rev. B 60 (1999) 773–777.
[32] T. Taniike, M. Tada, Y. Morikawa, T. Sasaki, Y. Iwasawa, J. Phys. Chem. B 110 (2006) 4929–4936.
[33] G. Gutierrez, A. Taga, B. Johansson, Phys. Rev. B 65 (2002), 012101-1-4.
[34] S.D. Mo, Y.N. Xu, W.Y. Ching, J. Am. Ceram. Soc. 80 (1997) 1193–1197.
[35] E. Menendez-Proupin, G. Gutierrez, Phys. Rev. B 72 (2005), 035116-1-9.
[36] M. Digne, P. Sautet, P. Rayboud, P. Euzen, H. Toulhoat, J. Catal. 226 (2004) 54–68.
[37] M. Digne, P. Sautet, P. Rayboud, P. Euzen, H. Toulhoat, J. Catal. 211 (2002) 1–5.
[38] M.C. Valero, P. Rayboud, P. Sautet, J. Phys. Chem. B 110 (2006) 1759–1767.
[39] M. Digne, P. Rayboud, P. Sautet, B. Rebours, H. Toulhoat, J. Phys. Chem. B 110 (2006) 20719–20720.
[40] H.P. Pinto, R.M. Nieminen, S.D. Elliott, Phys. Rev. B 70 (2004), 125402-1-11.
[41] A. Dyan, P. Cenedese, P. Dubot, J. Phys. Chem. B 110 (2006) 10041–10050.
[42] S. Cai, K. Sohlberg, J. Mol. Catal. A: Chem. 193 (2003) 157–164.
[43] G. Feng, C. Huo, C. Deng, L. Huang, Y. Li, J. Wang, H. Jiao, J. Mol. Catal. A: Chem. 304 (2009) 58–64.
[44] M. Sun, A.E. Nelson, J. Adjaye, J. Phys. Chem. B 110 (2006) 2310–2317.
[45] A.E. Nelson, M. Sun, J. Adjaye, J. Phys. Chem. B 110 (2006) 20724–20726.
[46] G. Paglia, C.E. Buckley, A.L. Rohl, J. Phys. Chem. B 110 (2006) 20721–20723.
[47] G. Paglia, C.E. Buckley, A.L. Rohl, B.A. Hunter, R.D. Hart, J.V. Hanna, L.T. Byrne, Phys. Rev. B 68 (2003), 144110-1-11.
[48] G. Paglia, A.L. Rohl, C.E. Buckley, G.D. Gale, Phys. Rev. B 71 (2005), 224115-1-16.
[49] L. Smrcok, V. Langer, J. Krestan, Acta Cryst. C62 (2006) i83–i84.
[50] H.A. Dabbagh, K. Taban, M. Zamani, J. Mol. Catal. A: Chem. 326 (2010) 55–68.
[51] A.D. Becke, J. Chem. Phys. 104 (1996) 1040–1046.
[52] C. Lee, W. Yang, R.G. Parr, Phys. Rev. B 37 (1988) 785–789.
[53] B. Delley, J. Chem. Phys. 92 (1990) 508–517.
[54] B. Delley, J. Chem. Phys. 113 (2000) 7756–7764.
[55] E. Kim, P.F. Weck, S. Berber, D. Tománek, Phys. Rev. B 78 (2008), 113404-1-4.
[56] http://www.iupac.org/goldbook/T06406.pdf.
[57] H. Knozinger, P. Ratnasamy, Catal. Rev. Sci. Eng. 17 (1978) 31–39.
[58] E.J.W. Verway, Z. Kristallogr. 91 (1935) 65–69.
[59] B.A. Hendriksen, D.R. Pearce, R. Rudham, J. Catal. 24 (1978) 82–87.
[60] S.V. Tsybulya, G.N. Kryukova, Phys. Rev. B 77 (2008), 024112-1-13.
[61] V. Shapovalov, T.N. Truong, J. Phys. Chem. B 104 (2000) 9859–9863.
[62] B. Shi, H.A. Dabbagh, B.H. Davis, J. Mol. Catal. A: Chem. 141 (1999) 257–262.
[63] H.A. Dabbagh, C.G. Hughes, B.H. Davis, J. Catal. 133 (1992) 445–460.
[64] H.A. Dabbagh, J. Mohammad Salehi, J. Org. Chem. 63 (1998) 7619–7627.
[65] B. Shi, B.H. Davis, J. Catal. 157 (1995) 359–367.
[66] M. Laroche, A. Pazderski, B. Blourt, Bull. Soc. Chim. Fr. (1968) 2541.
[67] B.H. Davis, J. Catal. 26 (1972) 348–351.
[68] H. Pines, C.N. Pillai, J. Am. Chem. Soc. 83 (1961) 3270–3274.
[69] G. Gutierrez, B. Johansson, Phys. Rev. B 65 (2002), 104202-1-9.
[70] H. Knözinger, H. Buhl, K. Kochloefl, J. Catal. 24 (1972) 57–68.
[71] H. Noller, K. Thomke, J. Mol. Catal. 6 (1979) 375–392.